



## *B* Physics at Hadron Colliders

J.N. BUTLER<sup>(1)</sup>

<sup>(1)</sup> *Fermi National Accelerator Laboratory, Batavia, IL, US*

**Summary.** — This paper discusses the physics opportunity and challenges for doing high precision *B* physics experiments at hadron colliders. It describes how these challenges have been addressed by the two currently operating experiments, CDF and DØ, and how they will be addressed by three experiments, ATLAS, CMS, and LHCb, at the LHC.

PACS 12.15, 14.65, 14.40, 14.20, 11:30 –  
PACS . – 11.30.

### 1. – Introduction

In this paper, we review the motivation for carrying out high statistics studies of the decays of particles containing *b*-quarks, emphasizing the decays of the  $B_s$ . We acknowledge the great contributions to our understanding of *B* physics from the  $e^+e^-$  *B*-factories but note their limitations. We then describe the challenges of performing high precision *B* physics studies at hadron colliders and identify the key elements of an experiment capable of extending the work that has already been done. We examine the response to these challenges by the two running general purpose experiments, CDF and DØ, at the Tevatron, and the prospects for *B* physics with the two general purpose detectors, CMS and ATLAS, at the LHC. We then look at the physics reach of the first “dedicated *B* hadron collider experiment,” LHCb.

We do not attempt to explain the physics of *B* decays. There have been excellent lectures on these topics at this School. We use selected results from CDF and DØ that have been presented at recent conferences [1] to illustrate the points we make.

### 2. – Physics Motivation

The purpose of the next generation of *B* physics experiments is to look for New Physics (NP) beyond the Standard Model (SM) in the CP-violating and rare decays of particles containing *b*-quarks. We know that there is New Physics because the Standard Model Higgs Boson is unstable to radiative corrections above the TeV scale; the baryon asymmetry of the universe is not explained; neutrinos have mass and large mixing angles; and there is no explanation for Dark Matter and Dark Energy.

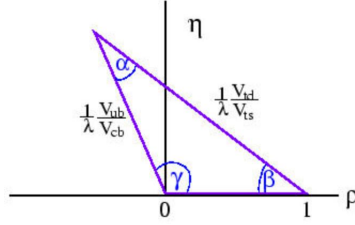


Fig. 1. – The CKM Triangle showing the angles  $\gamma$ ,  $\beta$ , and  $\alpha$  and their relation to the CKM Matrix elements  $V_{(t,c,u),(b,s,d)}$

There are many extensions of the SM. Nearly all of them contain arbitrary phases that could provide new sources of CP violation. The SM explanation of CP violation, based on the quark mixing, or CKM, matrix[2] is very prescriptive. If these new phases exist, they may produce deviations from the predictions of the SM.

There are three general approaches to searching for NP in  $B$  decays: 1) Precision determination of the CKM angles to look for small inconsistencies with the SM. This includes comparing the angles with predictions derived from measurement of the sides of the CKM triangle and making several “redundant” measurements of each angle in several processes that are predicted to be equivalent in the SM but are not necessarily so if there is NP; 2) Search for NP in quark mixing, especially of the  $B_s$  or due to new sources of CP violating asymmetries, especially as they appear in decays involving loop diagrams; and 3) New Physics amplitudes that contribute to rare decays and can either increase or decrease the decay rate predicted by SM.

**2.1. Precision Determination of CKM angles.** – The CKM matrix, written in Wolfenstein parametrization, has four parameters,  $\lambda$  (the sine of the Cabibbo Angle),  $A$ ,  $\rho$  and  $\eta$ [3]. The unitarity of the CKM matrix produces six equalities that can be represented as triangles in the  $\rho$ - $\eta$  complex plane. The CKM triangle most relevant to the discussion of  $B$  decays is shown in Fig. 1. The six CKM triangles can be written in terms of four independent angles[4]

$$(1) \quad \begin{aligned} \beta &= \arg\left(-\frac{V_{tb}V_{td}^*}{V_{cb}V_{cd}^*}\right) & \gamma &= \arg\left(-\frac{V_{ub}^*V_{ud}}{V_{cb}^*V_{cd}}\right) \\ \chi &= \arg\left(-\frac{V_{cs}^*V_{cb}}{V_{ts}^*V_{tb}}\right) & \chi' &= \arg\left(-\frac{V_{ud}^*V_{us}}{V_{cd}^*V_{cs}}\right) \end{aligned}$$

Of these angles, only  $\sin 2\beta$  has achieved the status of a precision measurement[5]. The angle  $\gamma$  is constrained by a variety of techniques[6] which are currently limited by statistics or by theoretical uncertainties. The angles are also constrained by measurements of the sides of the CKM triangle based on  $B$ -meson semi-leptonic decays and mixing. In the SM,  $\chi$  is predicted to be small and  $\chi'$  to be even smaller.

Table I gives a typical menu of decays of interest in challenging the consistency and adequacy of the CKM explanation of CP violation in  $B$  decays. The interest in making several measurements of quantities such as  $\beta$  and  $\gamma$  is that NP could couple to the various decays differently, spoiling the equality required by the SM. The requirements on the next generation of  $B$  experiments will be driven by the need to make high precision

TABLE I. – *Some Key Measurements of the CKM Matrix in B Decays*

Physics Quantity	Decay Modes
$\sin(2\alpha)$	$B^0 \rightarrow \rho\pi \rightarrow \pi^+\pi^-\pi^0$
$\cos(2\alpha)$	$B^0 \rightarrow \rho\pi \rightarrow \pi^+\pi^-\pi^0$
$\text{sign}(\sin(2\alpha))$	$B^0 \rightarrow \rho\pi, B^0 \rightarrow \pi^+\pi^-$
$\sin(\gamma)$	$B_s \rightarrow D_s K^-$
$\sin(\gamma)$	$B^+ \rightarrow D^0 K^+$
$\sin(\gamma)$	$B \rightarrow K\pi$
$\sin(\gamma)$	$B \rightarrow \pi^+\pi^-, B_s \rightarrow K^+K^-$
$\sin(2\chi)$	$B_s \rightarrow J/\psi\eta', J/\psi\eta, J/\psi\phi$
$\sin(2\beta)$	$B^0 \rightarrow (J/\psi, \psi')(K_s, K^*(K_s, \pi^0))$
$\sin(2\beta)$	$B^0 \rightarrow \phi K_s, \eta' K_s$
$\cos(2\beta)$	$B^0 \rightarrow J/\psi K^*, B_s \rightarrow J/\psi\phi$
$x_s$	$B_s \rightarrow D_s \pi^-$
$\Delta\Gamma$ for $B_s$	$B_s \rightarrow J/\psi\eta^{(\prime)}, J/\psi\phi, K^+K^-$

measurements of states such as the ones in this table. A number of these decays involve  $B_s$  and are therefore not accessible to  $e^+e^-$  machines designed to run on the  $\Upsilon(4S)$  and a number of these decays involve states containing photons, so that good electromagnetic calorimetry is required.

One way of checking the consistency of the CKM picture [7], [8], is through a measurement of the mixing-assisted CP asymmetry  $\sin 2\chi$ . This can be done, for example using  $B_s \rightarrow J/\psi\eta^{(\prime)}$ , where  $\eta \rightarrow \gamma\gamma$  and  $\eta' \rightarrow \rho\gamma$ . It is also possible to use  $B_s \rightarrow J/\psi\phi$ , which is somewhat easier to detect experimentally but requires a detailed angular analysis to extract  $\chi$ . The critical check is:

$$(2) \quad \sin \chi = \lambda^2 \frac{\sin \beta \sin \gamma}{\sin(\beta + \gamma)}$$

Given what we know about  $\beta$  and  $\gamma$ ,  $\chi$  is expected to be about  $2^\circ$  so a lot of data must be taken to measure this quantity.

**2.2. Search for New Physics in Rare B decays.** – Within the SM, decays are suppressed if they only have loop (Penguin) diagrams or loop diagrams and CKM-disfavored tree diagrams. New particles can appear in the loops and modify their decay characteristics. New physics could include new fermion-like objects or new gauge-like objects. Supersymmetry (SUSY) and left-right models are among the many that contain such particles.

In particular, decays dominated by the loop processes  $b \rightarrow (s, d)q\bar{q}$  may exhibit large deviations from SM predictions. These processes are illustrated in Fig. 2, which shows how SUSY can contribute to these decays. The decays involving  $b \rightarrow s\bar{s}$  have been studied intensively in the  $e^+e^-$  B-factories. They measure  $\sin 2\beta$  in these decays, which according to the SM, should be the same as measured in the CKM-favored tree-level decay  $B^0 \rightarrow \psi K_s$ . It is still unclear whether there are any statistically significant deviations[9]. More sensitive measurements are clearly needed.

Decays involving the ElectroWeak Penguins can be examined in detail for non-SM effects. Figure 3 shows predictions of the Forward-Backward asymmetry,  $A_{FB}$ , of the muon in the decay  $B^0 \rightarrow K^*\mu^+\mu^-$  as a function of the dimuon invariant mass squared,  $s$ . The SM predicts a zero in  $A_{FB}$  near  $3 \text{ GeV}^2$ , whereas in some NP models there is no zero at all[10].

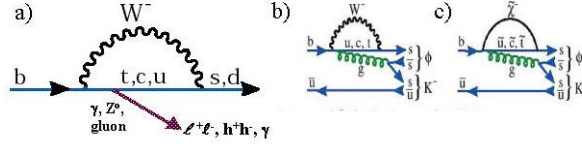


Fig. 2. – The  $b \rightarrow (s, d)$  loop. (a) shows the loop in the SM. The particles in the loop can radiate  $\gamma$ 's,  $Z$ 's, or (from the quark line) gluons. (b) shows the decay  $B^- \rightarrow \phi K^-$  in the SM. (c) shows the how SUSY can contribute to this decay mode.

Figure 4 illustrates how NP, in this case SUSY particles, can alter the mixing rate for the  $B_s$ . The righthand part of the figure shows the decay  $B_s \rightarrow J/\psi \eta$ . The mixing-assisted CP violation of this decay gives  $\sin 2\chi$ . In the SM, it is small because the dominant contribution to mixing,  $V_{ts}$ , does not have an imaginary part. However,  $V_{cs}$  and  $V_{ub}$  have imaginary parts giving rise to a small effect. NP, such as a SUSY contribution to mixing, shown in the middle entry in Fig. 4, could introduce additional phases. If these are large enough, the “apparent value” of  $\chi$  could be changed and the relation given in equation 2 would not be satisfied.

### 3. – Why do we need MORE than the $e^+e^-$ Asymmetric $B$ Factories?

The  $B$  factories have produced higher luminosities than even their most optimistic proponents believed possible. Typical luminosities are now  $1.5 \times 10^{34}/\text{cm}^2\text{-s}$  and may rise to  $10^{35}$ . The  $B$  factories at the  $\Upsilon(4S)$  produce only  $B^0 - \bar{B}^0$  and  $B^+ B^-$ . Still, many key CPV studies are statistics limited and many rare decays simply require more  $B$  production than will ever be achieved.

New approaches to CP asymmetries have made the  $B$  factories more capable of extracting the CP angles  $\alpha$  and  $\gamma$ . CP violation in  $B_s$  decays remains a source of important information through  $B_s$  mixing and the measurement of  $\gamma$  in  $D_s K$  decays is a crucial consistency check of the CKM picture. There are many other aspects of  $B$  physics that cannot be addressed at an  $e^+e^-$  collider operating at the  $\Upsilon(4S)$ . These include the study of  $b$ -baryons,  $B_c$  mesons, and very rare decays of  $B_d$ ,  $B_u$  and  $B_s$ .

What really counts, however, is the efficiency  $\times$  number of  $B$ 's (of specified type) produced and the ability to see signals above potentially large backgrounds. Efficiency is

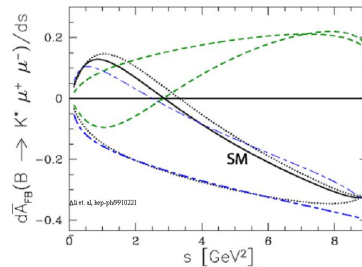


Fig. 3. –  $A_{FB}$ , the forward-backward muon charge asymmetry in the decay  $B^0 \rightarrow K^* \mu^+ \mu^-$  as a function of the dimuon invariant mass squared,  $s$ .

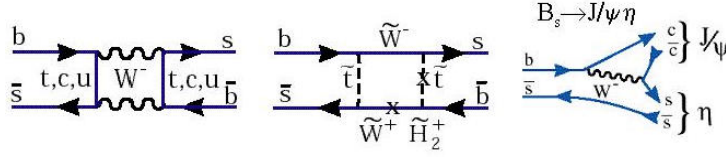


Fig. 4. – (left side) The box diagram that is responsible for  $B_s$  mixing in the SM; (Middle) A box diagram involving SUSY particles that could modify  $B_s$  mixing. (Right side) The decay diagram for  $B_s \rightarrow J/\psi\eta$  that, through its interplay with  $B_s$  mixing, gives  $\sin 2\chi$ .

the strong point of the  $e^+e^-$   $B$  Factories. The number of  $B$ 's produced is the strength of the hadron colliders. **The challenge for detectors at hadron colliders is to achieve high efficiency for reconstructed  $B$ 's and their flavor tags, while keeping the backgrounds under control.**

**4. –  $B$  Physics at Hadron Colliders**

The Tevatron, at a luminosity  $10^{32}/\text{cm}^2\text{-s}$ , produces  $10^{11}$   $b$ -pairs per year. Because a gluon from each beam particle collides to produce the  $B$ 's, the interaction is intrinsically asymmetric so time evolution studies are possible. Thus, it is a “Broadband, High Luminosity B Factory”, giving access to  $B_d$ ,  $B_u$ ,  $B_s$ ,  $b$ -baryon, and  $B_c$  states. Plans are in the works to increase the luminosity of the Tevatron to at least  $3 \times 10^{32}$ . Cross sections at the LHC will be 5 times larger and the luminosity will be much higher. Table II compares  $B$  production at various machines.

The  $b$  events are accompanied by a very high rate of background or “minimum bias” events. The  $b$ 's are produced over a very large range of momentum and angles. Even in the  $b$  events, there is a complicated underlying event so one lacks the strict constraints that one has in an  $e^+e^-$  machine. These lead to challenges in triggering, reconstruction efficiency, flavor tagging, and the background rejection.

**4.1.  $b$ -quark Production Mechanisms and Cross Sections at Hadron Colliders.** – The production mechanisms for particles containing  $b$ -quarks are shown in Fig. 5. The  $b\bar{b}$  cross section has been measured at the Tevatron by both CDF and DØ in the central rapidity region and for  $P_t$  ranging from a few GeV/c to 25 GeV/c[11],[12]. They are shown in Fig. 6 along with the theoretical predictions. Theory and experiment disagreed for a long period of time but with more data and better calculations, agreement is good[13].

TABLE II. –  $B$  Production at Various Machines

Facility	Luminosity $\text{cm}^{-2}\text{s}^{-1}$	$B$ pair cross section	Luminosity per year	$B$ pairs per year
FNAL Tevatron	$2 \times 10^{32}$	$100 \mu\text{b}$	$2 \text{ fb}^{-1}$	$2 \times 10^{11}$
$e^+e^-$ $B$ Factory ( $\Upsilon(4S)$ )	$3 \times 10^{34}$	$1.15 \text{ nb}$	$300 \text{ fb}^{-1}$	$3.45 \times 10^8$
LHC (early)	$1 \times 10^{33}$	$500 \mu\text{b}$	$10 \text{ fb}^{-1}$	$5 \times 10^{12}$
LHC (design)	$1 \times 10^{34}$	$500 \mu\text{b}$	$100 \text{ fb}^{-1}$	$5 \times 10^{13}$
LHCb (rate limited)	$2 \times 10^{32}$	$500 \mu\text{b}$	$2 \text{ fb}^{-1}$	$1 \times 10^{12}$

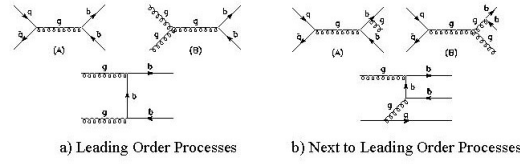


Fig. 5. – Mechanisms for producing particles containing  $b$ -quarks.

Also shown in Fig. 6 is the  $B$  cross section as a function of center-of-mass energy for the total cross section, the  $b\bar{b}$  and  $c\bar{c}$  cross section, and cross sections for many other important processes[14]. The cross section, extrapolated over all  $\eta$  and  $P_t$  comes out to about  $100 \mu\text{b}$  at the Tevatron and is calculated to be about a factor of 5 larger,  $\sim 500 \mu\text{b}$ , at the LHC. Although these cross sections, along with actual (Tevatron) or expected (LHC) machine performance, result in very high rates of produced  $B$ 's,  $B$  production is still a small fraction of the total cross section, leading to the challenges noted above.

**4.2.  $B$  Production Characteristics.** – There are several aspects of  $B$  production that impact experiment design at hadron colliders. Fig. 7 shows the distribution of  $\frac{P}{M_B}$  (or the product of the relativistic quantities  $\beta\gamma$ ) as a function of the pseudorapidity,  $\eta$ . The lifetime in the laboratory frame is proportional to this quantity. In the central region,  $\eta < 1.0$ , the average value of  $\beta\gamma$  is about the same as in the asymmetric  $e^+e^-$   $B$ -factories. At high  $\eta$ , in the forward direction with respect to the beams, the momenta are much higher. The  $B$ 's are produced over a large range of momenta and some of them travel a

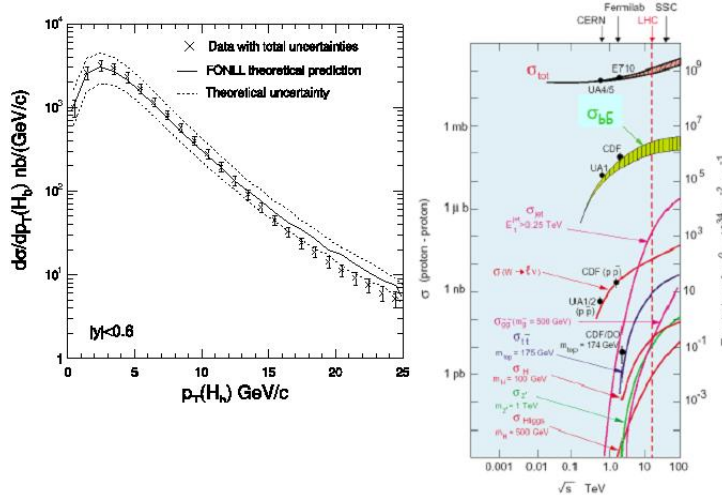


Fig. 6. – The left side shows the cross section for  $b - \bar{b}$  pairs at a center-of-mass energy of 1.96 TeV, in the central rapidity region  $|y| < 0.6$ , vs.  $P_t$  from CDF and DØ. The right side shows the cross sections as a function of  $\sqrt{s}$ , the energy in the center of mass, for many physics processes, including  $b$ -pair production.

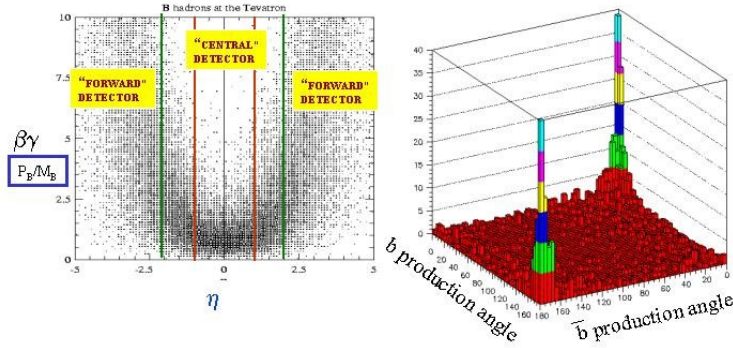


Fig. 7. – The left side shows the correlation of the  $\beta\gamma$  or momentum of the  $B$  particle with the pseudorapidity  $\eta$  at which it is produced. The right side shows the correlation between the polar angle of the  $B$  particle and the  $\bar{B}$  particle.

long distance ( $\sim 1\text{mm}$ ) before they decay.

Fig. 7 also shows another important correlation. While the polar angles of the  $B$  and the  $\bar{B}$  are not very correlated in the central region, they are strongly correlated in the forward (or backward) region. At high  $\eta$ , the two  $B$ 's tend to go in the same direction, either both forward or both backward. This is a result of the collision being between two gluons. The gluon-gluon center of mass is boosted in the direction of the more energetic gluon. The  $x$ -distribution of the gluons favors production of  $b - \bar{b}$  pairs of fairly low invariant mass. This correlation is of crucial importance to the design of hadron collider  $B$  experiments. A forward spectrometer covering only one side of the interaction region will still have high acceptance for both the “signal particle,” the one whose decay is being studied, and the “tagging particle.”

The azimuthal angle of the  $B$  relative to the  $\bar{B}$ , viewed in the plane perpendicular to the beam direction, tends to be peaked at  $180^\circ$ , although not as sharply as leading order calculations predict[15]. Higher order corrections modify these predictions.

At hadron colliders, all species of particle containing  $b$ -quarks are produced. Because of our lack of knowledge of absolute branching fractions for  $B_s$  and  $\Lambda_b$  decays, we still rely on the predictions of event generators, such as Pythia[16], for production ratios. The expected particle ratios are  $B_d \sim 40\%$ ,  $B_u \sim 40\%$ ,  $B_s \sim 10\%$ ,  $b$ -baryon  $\sim 10\%$ , and  $B_c \sim 0.1\%$ .

In addition to the two  $B$  hadrons, there are fragmentation products that are generated as the  $b$ -quarks are transformed into hadrons and there is a complicated underlying event from the remnants of the incoming and outgoing beam particles after the collision. Thus, many more particles than just the daughters of the  $B$  decays will be detected.

## 5. – Requirements for $B$ Physics Experiments at Hadron Colliders

The requirements for a hadron collider  $B$  experiment are driven by the nature of  $B$  production described above, the characteristics of the parent  $B$  (e.g.  $B_{d,u}$  or  $B_s$ ) and the decay modes (e.g final state, branching fraction) to be studied, and the details of the analysis to be performed (time evolution, tagged study, Dalitz or angular analysis). The decays listed in Table I are a representative set that can be used to set these requirements.

One requirement is the capability to isolate the  $B$  decay signals from the potentially

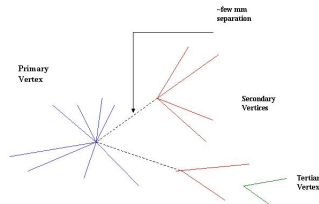


Fig. 8. – Vertex topology of a  $B$  event. This event represents a typical event in the forward region where the  $B$  and  $\bar{B}$  tend to go in the same direction with respect to the beam.

large backgrounds, including combinatoric backgrounds from so-called “minimum bias” or light-quark events that contain no  $b$ -quark states, and from the underlying event or the second  $B$  in a true  $b$ -quark event.

Precision tracking based on silicon strip microvertex detectors or silicon pixel detectors is powerful enough to reconstruct the primary and all secondary and tertiary vertices that occur in an event with produced  $B$ 's. A typical vertex topology is shown in Fig. 8. In addition, many of the key studies involve the measurement of differences in the time evolution of the  $B$ 's as they move away from the primary vertex and eventually decay. The same vertex detector that is used to reconstruct the vertices is also able to measure the spatial separation between the primary and signal  $B$  decay vertex.

A typical approach to background reduction is to associate tracks with vertices, identify the primary vertex and the secondary  $B$  vertex candidate, then compute the separation of the vertices,  $L$ , and its uncertainty,  $\sigma_L$ . One can then cut on the ratio,  $L/\sigma_L$  to reduce the background. This allows the isolation of just those particles that are the daughters of a  $B$  decay of interest, virtually eliminating background from non- $B$  events and greatly reducing combinatoric background within  $B$  events. Figure 9 shows the  $L/\sigma_L$  distribution for  $J/\psi$ 's from  $B$  decays and those coming from the primary vertex. A cut of  $L/\sigma_L$  of 3 or 4 reduces the background effectively and reduces the signal efficiency only slightly. The  $L/\sigma_L$  distribution for  $B_s \rightarrow D_s K$  is shown in Fig. 9c.

The quantity  $L$ , together with the reconstructed momentum of the signal  $B$  allows the measurement of the proper time of the decay. Modern vertex detectors achieve spatial resolutions of  $10 \mu\text{m}$  or better, which results in proper time resolutions that range from  $35 \text{ fs}$  to  $50 \text{ fs}$  depending on the final state. If the requirement for vertex resolution was driven by the need to reduce backgrounds and measure  $B$  lifetimes, this would be overkill. However, it is driven instead by the need to measure  $B_s$  mixing whose period is expected to be only a few hundred  $\text{fs}$  but could be less, and to follow the rapid oscillations to

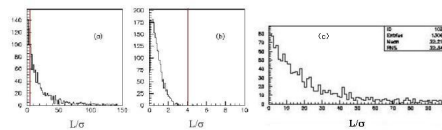


Fig. 9. – (a) The  $\frac{L}{\sigma_L}$  for  $J/\psi$ 's from  $B$  decays; (b) The  $\frac{L}{\sigma_L}$  for  $J/\psi$ 's coming from the primary vertex. Note that these distributions are not normalized to a constant luminosity. Nevertheless, it is clear that vertex detachment is a powerful discriminant between  $B$  signals and backgrounds. (c) The distribution in  $L/\sigma_L$  for  $B_s \rightarrow D_s K$  in a typical forward spectrometer [17]

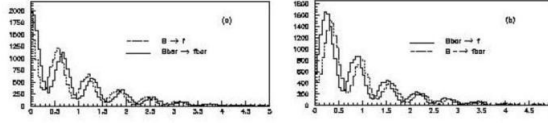


Fig. 10. – Proper time distribution for  $B_s$  decaying to a non-charge conjugate state,  $f$ , assuming  $X_s \equiv \Delta m_s/\Delta\Gamma = 20$  a)  $B_s \rightarrow f$  and  $\bar{B}_s \rightarrow \bar{f}$ ; and b)  $\bar{B}_s \rightarrow f$  and  $B_s \rightarrow \bar{f}$ .

extract CP asymmetries in  $B_s$  decays, shown in Fig. 10. Excellent proper time resolution is also necessary to measure the difference in lifetime between the two CP eigenstates of the  $B_s$ , called  $B_s^H$  and  $B_s^L$ . This difference is expected to be about 150-200  $f_s$ .

A second powerful tool for isolating the signal and rejecting background is the precise reconstruction of the momentum of charged particles. This allows reconstruction of the invariant mass of the signal  $B$  from the momentum measurements of the decay's daughter particles. A cut on the mass will eliminate errant associations. Another important reason for good momentum and mass resolution is that several of the decays of  $B$  mesons and  $b$ -baryons of interest contain  $K_s$ 's and  $\Lambda$ 's that decay into  $\pi^+\pi^-$  and  $\pi^-p$ , respectively. However, many of these decays occur outside of the vertex detector and are reconstructed only by the main magnetic spectrometer. A typical mass resolution for a complicated final state such as  $B_s \rightarrow D_s^- K^+$  where the  $D_s^- \rightarrow \phi\pi^+$  and  $\phi \rightarrow K^+K^-$  can be as good as  $\sim 10$ -15 MeV/ $c^2$  in a forward rapidity region detector.

Another important element required for a capable  $B$  detector is a particle identification system that can cover a wide range of momenta. Particle identification helps identify the final states of interest. Without good particle identification, false mass hypotheses smear other signals in mass and produce background under the mass peak of the signal decay. This turns out to be especially bad for two body states where “reflections” from  $B$  decays that are not part of the study may, due to mass misassignments, fall into the mass interval of interest. In some cases, they even form a peak in the vicinity of the signal. Figure 11 shows how mass misassignments in the two body decays of  $B_d$  and  $B_s$  can result in such reflections and demonstrates how capable particle identification based on Ring Imaging Cherenkov Counters can eliminate this problem[18].

Another requirement of any detector intended to study  $B$  physics is “flavor tagging” capability. Due to mixing, a produced  $B$  meson may turn into a  $\bar{B}$  meson and decay from that state. The interference of mixed decays and direct decays is an important source of CP violation. It is important to determine the “flavor” with which the original signal  $B$  meson was produced. There are two ways of achieving this, called “away-side” tagging and “same-side” tagging.

“Away-side” tagging is based on the idea that the “signal particle” is produced with the opposite flavor of the “other”  $B$  in the event. If the flavor of that other  $B$  can be determined, then the flavor of the signal decay is also known. This process has several difficulties that result in mislabeling the away-side flavor. The methods used to identify the flavor of the away-side  $B$  are lepton tagging from semileptonic decays, jet charge tagging of the “away-side” secondary vertex, and charged kaon tagging. The kaon typically comes from the decay of a charmed daughter of the away-side  $B$ . Kaon identification over a wide momentum range, applied to particles that don't come from the primary vertex, is one of the most effective tools for away-side tagging.

“Same-side” tagging[19] involves a correlation between the flavor of a signal  $B$  decay

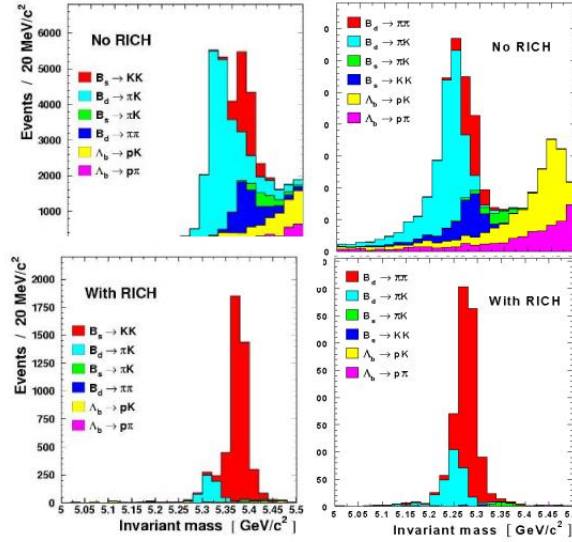


Fig. 11. – This figure shows the need for charged hadron particle identification. The upper right hand figure is a search for  $B^0 \rightarrow \pi^+\pi^-$ . It shows a typical spectrum of detached two-body decays with all particles assigned the pion mass, i.e. with no particle identification. There are severe backgrounds from misassignment of particle types which “reflects” other states into the  $B^0$  mass region; The lower right hand figure shows what happens when only pions identified in the RICH system are included in the plot. The signal now has very little background. The left hand upper and left hand lower plots show the same situation for  $B_s \rightarrow K^+K^-$ .

and the charge of fragmentation products that are nearest it in rapidity. The origin of this correlation is shown in Fig. 12. The correlation is especially strong for  $B_s$  decays. These fragmentation products come from the primary vertex. Good particle identification over a wide momentum range is crucial for this kind of tagging.

Another key requirement of an experiment to study the states typified by Table I is the ability to reconstruct neutrals in the harsh environment of a hadron collider. Many of the states involve photons from the decays of  $\pi^0$ 's,  $\eta$ 's, or  $\eta'$ 's. There are many photons in typical events and, given the techniques of photon detection, there is no easy way to isolate the ones that point to the signal  $B$  vertex from those that come from the primary vertex. Combinatorial backgrounds are therefore vicious. However, knowledge

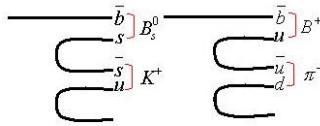


Fig. 12. – Schematic representation of the fragmentation process showing why the charged particle nearest the  $B_s$  in rapidity is usually a  $K^+$  and nearest a  $B^+$  is usually a  $\pi^-$ . This correlation can provide a “same-side” flavor tag.

of the direction of the  $B$  decay from the reconstruction of the primary vertex and the  $B$ (signal) vertex, reconstructed from its charged daughters, can be used to greatly reduce the number of photons that need to be considered as candidates for daughters of the decay. Segmentation is crucial because the detector must guard from being fooled by overlapping showers, including those from hadrons interacting in the electromagnetic calorimeter. Energy resolution is important to avoid combinatoric background in  $\pi^0$ ,  $\eta$ , and  $\eta'$  reconstruction and to preserve good mass resolution and momentum resolution when these states are included in  $B$  signals.

Because the total cross section at a hadron collider is 100-500 times the  $B$  rate, an experiment aimed at high statistics studies or the study of very rare decays must be able to tolerate very high collision rates. Since vertex detectors must be very close to the beams to achieve good resolution, the vertex detectors, and perhaps other detectors, must be radiation tolerant. This requirement extends to the electromagnetic calorimeter. The topic of radiation hard and radiation tolerant detectors is the subject of intensive R&D that is beyond the scope of this lecture[20].

The large rate of “typical interactions” compared to “interesting” ones leads to a severe triggering problem, which is usually addressed by a “hierarchical” trigger scheme[21]. Level 1 is usually has “fixed latency” and must inspect every beam crossing, almost always with specialized, custom trigger hardware. Latency is defined as the time between the beam crossing and the time when the trigger decision is returned to the front end electronics and readout can be started. It is the time during which data must be stored while the trigger decision is being made. Trigger decisions must be made at the beam crossing rate, but the time permitted to make each one is the latency, typically only a few microseconds. Level 2 deals with the much smaller number of events that have passed the Level 1 selection, and can take correspondingly longer. There is time for more advanced hardware (DSP’s, FPGA’s) or standard CPU’s to do more complex calculations. Level 2 may have fixed or variable latency and may have hundreds of microseconds or milliseconds to handle a single event. Level 3 deals with the even smaller number of events that have passed Level 2, and uses commercial off the shelf CPUs to do an almost full offline type analysis for the final selection. The final step in the process is to record promising candidate events for offline analysis.

Finally, because the actual rate of  $B$  events is high, easily amounting to several thousand events per second into the detector acceptance at the LHC or Tevatron, and it is desirable to record as many of them as possible, a high capacity, high throughput data acquisition system is a necessity.

The requirements for a detector that can run at a hadron collider to do high precision  $B$  physics may be summarized as:

- Ability to run at high luminosity with high efficiency and operate for long periods of time in high radiation fields without performance degradation;
- A magnetic spectrometer with good acceptance for  $B$  decays products (signal) and the particles used in flavor tagging and good momentum and mass resolution for isolating  $B$  signals;
- A radiation hard vertex detector with superb vertex resolution for background rejection and for measuring rapid oscillations and small lifetime differences in the  $B_s$  system;
- A very efficient trigger for a wide variety of “hadron-only” final states with “hadron-only” tags;

- An excellent particle identification system for charged hadrons, muons, and electrons to avoid kinematic reflections and to do efficient flavor tagging;
- Ability to reconstruct individual photons,  $\pi^0$ 's, and  $\eta$ 's, with high efficiency for studying the many interesting states containing neutrals; and
- A very high speed, high capacity data acquisition system.

## 6. – Central region vs Forward Region Detectors

Detectors designed to search for and study high mass particles or objects, such as Higgs and SUSY particles, jets, new quarks and new gauge bosons, which are produced in hard collisions, focus on the central rapidity region where the production and acceptance of these states is large. While plenty of  $B$ 's are also produced in this region, the solenoidal detectors that are optimum for high  $P_t$  physics in the central region lack several of the desirable attributes for detectors to study  $B$  physics.

In contrast, the forward region of rapidity offers longer decay lengths due to the large time dilation, lower multiple scattering, the availability of good particle identification techniques and the space along the beam direction needed to implement them. The photons from  $B$  decays have high energies for which electromagnetic calorimeters have good resolution.

Because of the interest in high mass physics, the detectors at the Tevatron cover the central region and were designed with high mass, high  $P_t$  physics as their priority. To study this physics, the detectors have solenoids that provide large acceptance, good mass and momentum resolution, and good muon and electron identification. They also have good vertex detectors that are essential for tagging  $b$ -jets produced in top quark decays and by many new high mass states. These provide CDF and DØ with many of the tools needed to do  $B$  physics, which has become an important goal of the current run. While the current detectors at the Tevatron still have difficulty competing with the  $e^+e^-$   $B$ -factories in the study of  $B_d$  and  $B_u$ , at present they are the only source of information on the decays of  $B_s$ ,  $B_c$  and  $b$ -baryons[22]. There has never been a dedicated  $B$  experiment at a hadron collider and there are now no longer any plans for one at the Tevatron.

This situation will change when the LHC turns on. In addition to their two high- $P_t$  detectors, CMS and ATLAS, that will have some capability to study  $B$  physics from  $B$ 's produced in the central region, there will be a “dedicated  $B$  physics experiment,” LHCb, that will cover the forward rapidity region. This will be the first experiment that is specifically optimized for studying  $B$  decays to take data at a hadron collider and is the only one now planned. The  $\eta$  and  $P_t$  of ATLAS, and CMS are approximately  $|\eta| < 2.5$  and  $P_t > 6$  GeV/c, whereas LHCb's coverage is approximately  $2 < \eta < 5$  and  $P_t > 2$  GeV/c.

One major difference between central and forward detectors is the quality of the charged hadron particle identification. Figure 13 illustrates the different capabilities of the particle identification in CDF[23] and LHCb[24]. LHCb has to cover a much larger range of momenta but can do so because of the extra space along the beam and the availability of the Ring Imaging Cherenkov technique.

## 7. – $B$ Physics at General Purpose Detectors at the Tevatron: Triggering

Triggering is one of the major challenges for any hadron collider  $B$  experiment. Only a small fraction of the collisions can be recorded to mass storage for subsequent physics

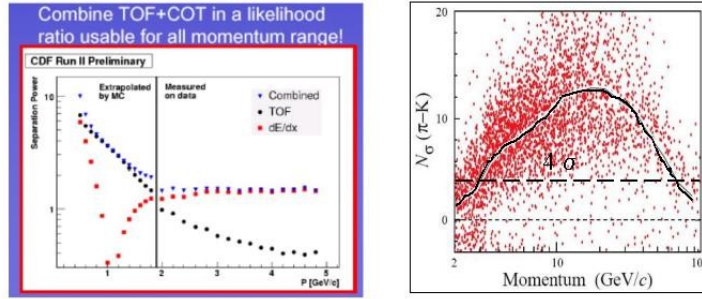


Fig. 13. – Comparison of the charged particle identification at CDF and LHCb: The left side shows the discrimination due to the time-of-flight system vs momentum in CDF; The middle shows the discrimination from the Time-of-Flight counters combined with  $dE/dx$  vs momentum in CDF. The right side shows the particle identification power of the RICH system in LHCb vs momentum.  $\pi$ -K separation is at least  $4\sigma$  over the whole range from 3 to 90 GeV/c.

studies. The trigger must choose the most important events for achieving the full range of physics goals of the experiment, including  $B$  physics. At the Tevatron, CDF and DØ trigger on  $B$ 's in different ways. CDF has relies on impact parameter triggers and DØ on muon triggers.

**7.1. CDF: The SVT Trigger and Illustrative Recent Results.** – CDF has implemented an “impact parameter” trigger to select events that have tracks with large impact parameters with respect to the primary interaction vertex. Such tracks are characteristic of the charged daughter particles of a  $B$  decaying downstream of the primary interaction. The trigger, called the “Silicon Vertex Trigger,” (SVT)[25], is based on the silicon microstrip vertex detector, shown in Fig. 14a. Figure 14b shows how the decay of a  $B$  results in tracks with a large, measurable impact parameter.

Because the time required to process an interaction is long and all the event data has to be stored while the trigger decision is being executed, the SVT takes place at Level 2 of the CDF trigger hierarchy. The Level 1 trigger selects  $B$  candidates with muons using its muon detector and with hadrons based on tracks with high transverse momentum,

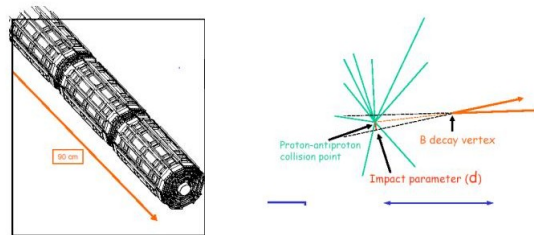


Fig. 14. – The left side is a schematic of the CDF Silicon Vertex Detector, the SVX; The right side is an illustration of the impact parameter due to the decay of a  $B$ .

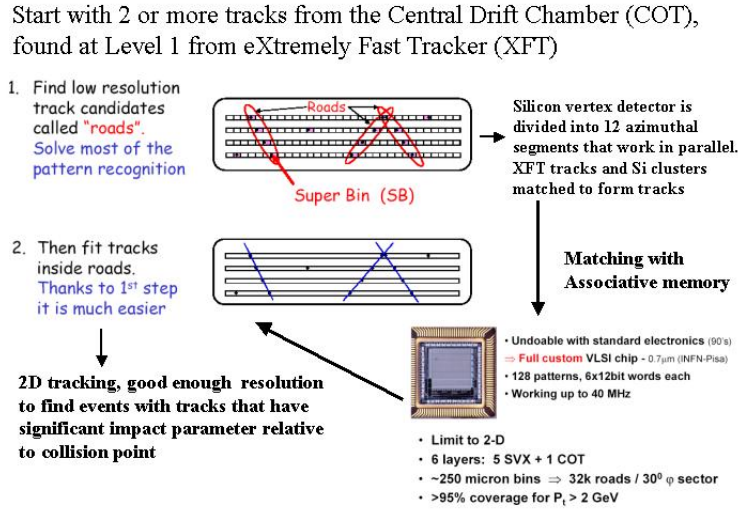


Fig. 15. – A summary of the implementation of the SVT algorithm.

based on a fast track reconstruction, the “eXtremely Fast Tracker” (XFT)[26] using its Central Drift Chamber. About 50,000 events per second, selected from almost 10 million collisions per second by the Level 1 trigger, can be processed by the SVT at Level 2.

The operation of the SVT is described in Fig. 15. The vertex detector is organized into “crude” roads based on groups of 5 microstrips. The roads are matched to tracks from the XFT, and the silicon detector hit clusters found inside the roads are then fit to form tracks. The fitting is done in 2 dimensions. This is accurate enough to find events that have high impact parameters relative to the colliding beam region, which has a  $\sigma$  of only about 35 $\mu$  m. The coverage is >95% for tracks with  $P_t >$  a few GeV/c.

Two key aspects of the SVT performance are the latency of the SVT calculation, which is typically about 24 $\mu$ s and the impact parameter resolution, which is 48 $\mu$ m, receiving approximately equal contributions from the size of the beam and the resolution of the SVT with this trigger algorithm.

The SVT information is used in conjunction with other trigger elements to form two sets of Level 2 triggers:

**Hadronic** Two SVT tracks with  $P_t > 2$  GeV/c,  $P_{t1} + P_{t2} > 5.5$  GeV/c, opposite charge,  $120 \mu\text{m} < d_o < 1$  mm and  $L_{xy} > 200 \mu\text{m}$ .

**Semi-leptonic** 1 lepton with  $P_t > \text{GeV}/c$  and 1 SVT track with  $P_t > 2$  GeV/c and  $120 \mu\text{m} < d_o < 1$  mm.

This trigger makes accessible to CDF a large variety of decays that have only hadrons in the final states, without relying on the away-side muon for triggering.

Vector-vector decays like  $B_s \rightarrow J/\psi(\mu^+\mu^-)\phi(K^+K^-)$  have both CP-odd and CP-even amplitudes. Since the CP even and odd states can have different lifetimes, the proper time distribution of the decay is a superposition of exponentials that can be

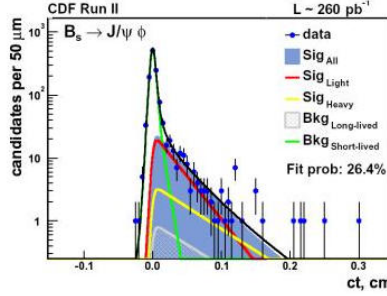


Fig. 16. – Decomposition of the time evolution of the decay of  $B_s \rightarrow J/\psi\phi$  into separate exponentials for the CP-even and CP-odd states of the  $B_s$ .

unfolded. Figure 16 shows a recent study of this decay by CDF[27]. They find

$$(3) \quad \frac{\Delta\Gamma_s}{\Gamma_s} = 0.65^{+0.25}_{-0.33}$$

This is a very sophisticated analysis and shows the power of hadron collider  $B$  experiments, even ones not designed specifically with  $B$  physics in mind.

Figure 17 shows a recent result for  $\Delta M_s$ , the  $B_s$  mixing parameter[28].  $B_s$  oscillations are predicted by theory to be much more rapid than  $B_d$  oscillations. In fact, so far only a lower limit on the oscillation frequency has been set. The world average lower limit is  $\Delta M_s \sim 14$ . The CDF result is based on combining results on hadronic and semileptonic decay modes. Also given in the figure is a projection of CDF’s sensitivity to  $B_s$  mixing as the integrated luminosity increases from  $\sim 1 \text{ fb}^{-1}$  that has been recorded so far in Tevatron Run 2 to  $4\text{--}8 \text{ fb}^{-1}$  expected over the remainder of the Tevatron’s life[29].

**7.2.  $D\bar{D}$ : The Muon Trigger and Illustrative Recent Results.** –  $D\bar{D}$  relies on muon triggers[30] to select  $B$  events. Their muon trigger has large coverage in pseudorapidity,  $|\eta| < 2$ , and has high efficiency for muons with  $P_t > 1.5 \text{ GeV}/c$ . A combination of single

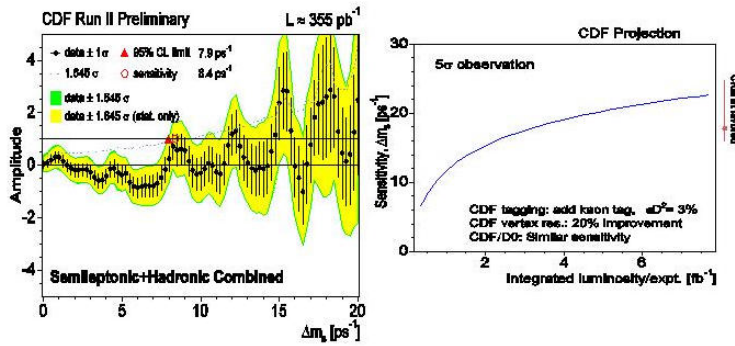


Fig. 17. – (left side) CDF result for determination of  $\Delta M_s$  using both semileptonic and hadronic decays. (Right side) Projection of CDF sensitivity to  $\Delta M_s$  as a function of integrated luminosity, assuming improvements in tagging efficiency and vertex resolution.

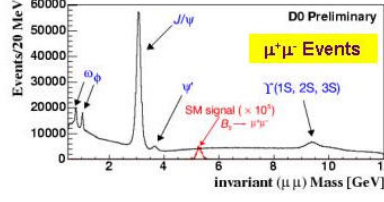


Fig. 18. – Spectrum of oppositely signed dimuons in  $D\bar{0}$  showing all the established two-body resonant states with branching fractions into this mode.

muon and dimuon triggers is employed. Above a few  $\text{GeV}/c$ , the triggered sample has very high purity, with over 65% of the triggers coming from events containing  $B$ 's. This trigger has enabled  $D\bar{0}$  to carry out studies of decays containing dimuons,  $J/\psi$ 's where the  $J/\psi \rightarrow \mu^+\mu^-$ , and semileptonic decays. Purely hadronic final states can be studied when the “away side”  $B$  has a muon or dimuon in its final state. Figure 18[31] shows the mass spectrum of opposite signed dimuons up to an invariant mass of  $12 \text{ GeV}/c^2$ . Figure 19 shows searches for the rare decays  $B_s \rightarrow \mu^+\mu^-$  and  $B_s \rightarrow \mu^+\mu^-\phi$ [32]. The resulting limits are given in Table III

$D\bar{0}$  has also made a measurement of  $\Delta\Gamma_s$  [32] based on the decay  $B_s \rightarrow J/\psi(\mu^+\mu^-)\phi$ , where  $\phi \rightarrow K^+K^-$ . The measurement employs an angular analysis, based on so-called “transversity” variables, together with the proper time distribution of the decay to separate the CP-even and CP-odd components of the decay. The angular distributions and the proper time distributions are shown in Fig. 20. The lifetime difference is found to be

$$(4) \quad \frac{\Delta\Gamma_s}{\Gamma_s} = 0.21_{-0.40}^{+0.27} \pm 0.20$$

This is based on  $460 \text{ pb}^{-1}$ . It will improve dramatically as more statistics are added using data already in hand and as more data are accumulated.

$D\bar{0}$  also produced a limit for  $\Delta M_s$ [32]. Their preliminary lower limit is  $\Delta M_s > 5.0 \text{ ps}^{-1}$ . This is well below the world average lower limit and the range of values expected in the SM (20-28) but it will improve because there will be much more data, modifications are being made to the detector and trigger, and analysis techniques will improve. The projected reach of  $D\bar{0}$  for  $\Delta M_s$  is shown in Fig. 21[32].

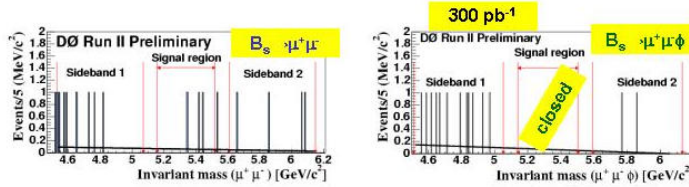


Fig. 19. – The left side shows the invariant mass spectrum of  $\mu^+\mu^-$  that are detached from the primary vertex in the vicinity of the  $B_s$  mass; the right side shows the invariant mass spectrum of  $\mu^+\mu^-\phi(\rightarrow K^+K^-)$  that are detached from the primary vertex in the vicinity of the  $B_s$ .

TABLE III. –  $D\bar{O}$  Limits for Rare  $B_s$  Decays containing Dimuons

Channel	BR Limits (95% CL)	SM Prediction
$\mu^+\mu^-$	$3.7 \times 10^{-7}$	$3.4 \times 10^{-9}$
$\mu^+\mu^-\phi$	$1.2 \times 10^{-5}$	$1.6 \times 10^{-6}$

## 8. – $B$ Physics at the LHC

8.1. *B Physics with the General Purpose Detectors ATLAS and CMS.* – ATLAS and CMS are “general purpose” detectors designed to discover NP in high mass at the energy frontier. Goals include the detection and study of Higgs, SUSY, new vector bosons, new fermions, leptoquarks, and new dynamics. Both detectors are designed to reconstruct the basic objects that would be produced by NP: high transverse momentum electrons, photons, muons,  $\tau$ 's, and jets. Among the jets are those containing  $B$ 's. Consequently, the detectors are, like CDF and  $D\bar{O}$ , equipped with many features that enable them to do some  $B$  physics[33], including silicon vertex detectors - needed for tagging  $b$  and  $\tau$  jets that are prominent signatures of NP, muon detectors, and electron/photon detectors. However, they lack particle identification and have very limited capability to trigger on  $B$ 's, relying mainly on single muon and dimuon triggers.

The beam crossing rate at the LHC is 40 MHz and nearly every crossing contains many collisions. Because of this, the first level trigger must operate with very low latency and must be simple. The workhorse trigger for  $B$  physics in both CMS and ATLAS is the muon trigger. Figure 22[34] shows the  $P_t$  of the muons from different sources. Above  $P_t$  of 6 GeV/c, the muon rate is dominantly from  $B$  decays. At a “low” luminosity of  $10^{33}/\text{cm}^2\text{-s}$ , single muon and dimuon triggers will be used. At “high luminosity” of  $10^{34}$ , probably only dimuon triggers will be feasible.

For vertex reconstruction, both CMS and ATLAS have silicon pixel detectors. Pixel detectors are more radiation-hard than silicon microstrips and are therefore more suitable to be stationed close to the colliding beams. They enable ATLAS and CMS to identify  $b$ -jets and  $\tau$ 's based on charged members of the jets having impact parameters relative to the beam or by the presence of secondary vertices. They also enable the identification

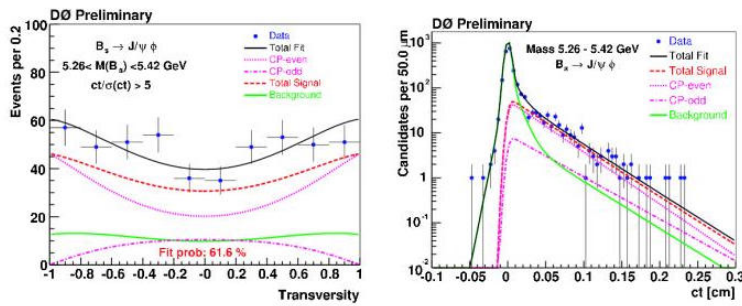


Fig. 20. – The left hand plot shows the distribution of the cosine of the transversity angle along with the shape for CP-even and CP-odd decays; the right hand plot shows the proper time distribution of the decay showing the data and the fitted results for the CP-even and CP-odd components from which the lifetime difference is obtained.

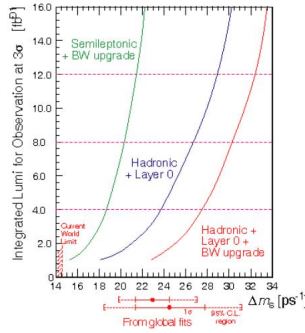


Fig. 21. – Expected evolution with integrated luminosity of  $DØ$ 's sensitivity to  $B_s$  mixing. Three projections are shown. The leftmost curve is based on using semi-leptonic decays but with upgraded bandwidth into the Level 3 farm; The middle curve assumes the addition of a new layer of silicon tracker, called Layer 0, very near the beam, and the use of hadronic decay modes; the rightmost curve is the projection with all three improvements.

of  $B$  mesons and baryons by secondary vertex reconstruction. The CMS pixel detector is shown in Fig. 23[35].

CMS and ATLAS both will have severe problems in triggering on  $B$ 's. At a “modest” luminosity of  $10^{33}/\text{cm}^2\text{-s}$ , the event rate is 100MHz and the rate of  $B$  production is 500KHz! The allowed rate of output to archival storage after all trigger levels is at best a few hundred Hz in each experiment. The menu of high  $P_t$  “discovery physics” is large and may not easily fit into the available output bandwidth.  $B$  events must compete with events that satisfy the signatures for a wide variety of NP. There will be a strong tendency, also already apparent in CDF and  $DØ$ , to squeeze out the  $B$  triggers in favor of higher priority physics.  $DØ$  and CDF are both increasing their triggering and output capabilities to preserve their  $B$  physics as the luminosity of the Tevatron increases.

With this in mind, ATLAS and CMS expect to focus on  $B$  states with muons and

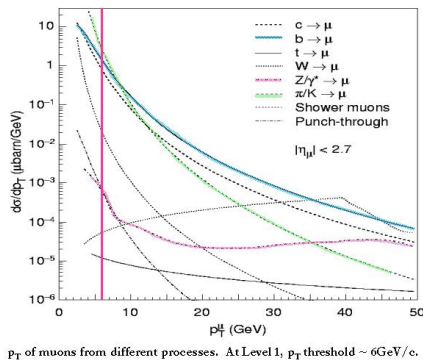


Fig. 22. – The  $P_t$  spectrum of muons expected from various sources at the LHC as calculated by the ATLAS collaboration.

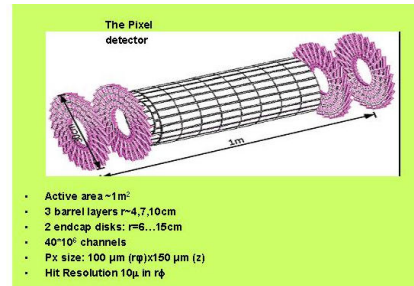


Fig. 23. – The CMS Pixel Detector.

TABLE IV. – *The Program of B Physics at ATLAS*

CP Violation	$B_d \rightarrow J/\psi(ee)K_s^0(\pi\pi)$ $B_d \rightarrow J/\psi(\mu\mu)K_s^0(\pi\pi)$ Control Channel: $B^+ \rightarrow J/\psi(\mu\mu)K^+$ $B_d \rightarrow J/\psi(\mu\mu)K^{*0}(K^+\pi^-)$	$\sin 2\beta$
	$B_s \rightarrow J/\psi(\mu\mu)\phi(KK)$ $B_{d,s} \rightarrow J/\psi(\mu\mu)\eta(\gamma\gamma)$	$\Delta\Gamma_s = \Gamma_H - \Gamma_L; \Gamma_s; A_{  }; A_{\perp}$ ; the strong phase differences $\delta_2 - \delta_1$ ; the weak phase $\phi_s$
Measurement of $B_s$ oscillations	$B_s \rightarrow D_s\pi; B_{s,d} \rightarrow D_s a_1$ $D_s^- \rightarrow \phi\pi^-; \phi \rightarrow K^+K^-$	$\Delta m_s = m_H - m_L$
Rare Decays	$B_{s,d} \rightarrow \mu^+\mu^-; B_d \rightarrow K^{*0}\mu^+\mu^-$ $\Lambda_b \rightarrow \Lambda\mu\mu; B_s \rightarrow \phi\mu\mu$	Precise measurements of the Branching Ratio
$\Lambda_b$ polarization measurements	$\Lambda_b \rightarrow J/\psi(\mu\mu)\Lambda(p\pi)$	Asymmetry parameter $\alpha_b, P_b$ , lifetime measurements
$B_c$ mesons	$B_c \rightarrow J/\psi\pi; B_c \rightarrow J/\psi\mu\nu$	Precise determination of $B_c$ mass and $B_c$ lifetime

dimuons, which they can trigger on efficiently and which have high purity. A possible menu of  $B$  physics that can be done in association with a program of discovery physics is given for the ATLAS experiment in Table IV[34]. As the luminosity increases it will be harder to preserve a meaningful share of the trigger and output bandwidth for  $B$  physics. The number of interactions per crossing will increase to  $\sim 25$ , which will probably lead to increased backgrounds. Moreover, the inner layers of the pixel detectors will suffer radiation damage and their performance will begin to degrade after a few years of LHC operation, resulting in poorer resolution and more background. For these reasons, it is likely that  $B$  physics will be done in the early years of ATLAS and CMS running but may decline in importance after a few years. If the vertex detectors continue to function at the highest luminosities, the emphasis will be on the search for very rare decays that contain dimuons.

**8.2. A Dedicated B Physics Experiment - LHCb.** – LHCb is a dedicated  $B$  physics experiment planned for the LHC[36]. It covers a range of angles from about  $\pm 15\text{ mrad}$  to about  $\pm 300\text{ mrad}$  with respect to the proton beams. It covers only one side of the interaction region (IR), relying on the angular correlation noted above to detect both the “signal  $B$ ” decay and the “tagging  $B$ ” fragments. It will be the first detector at a hadron collider whose design is optimized for  $B$  physics.

A schematic layout of LHCb is given in Fig. 24. Near the Interaction Point(IP), it has a precision vertex detector [37], the “Vertex Locator” or “VELO,” shown in Fig. 25 It consists of silicon microstrips in an  $r$ - $\phi$  arrangement especially suited for making a secondary vertex trigger that is described below. This is followed by an Aerogel Ring Imaging Cherenkov counter[24], RICH1, that provides particle identification from  $125\text{ mrad}$  to  $300\text{ mrad}$ . Two silicon microstrip tracking chambers, called the “trigger tracker” follow RICH1. They have a pitch of  $200\ \mu\text{m}$ . They are used in the trigger. A large, tapered dipole magnet provides a strong magnetic field,  $\int B \times dl = 4\ \text{T}\cdot\text{m}$ , for momentum analysis. Straw tube chambers provide downstream tracking for the momentum measurement. Following that is a second gas Ring Imaging Cherenkov detector, RICH2, providing particle

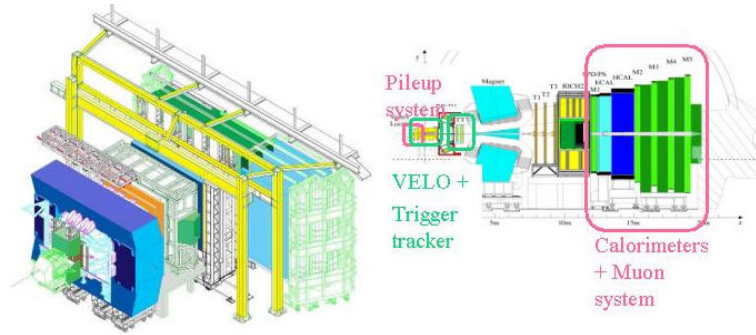


Fig. 24. – (left) a 3-D picture of the the LHCb detector; (right) a plan view.

identification from  $15 - 125mr$ . Together the two Cherenkov counters cover the momentum range from a few GeV/c up to 100 GeV/c. A pre-radiator and lead-scintillator Shashlik-style calorimeter (ECAL) provide photon reconstruction and electron identification. The ECAL is used in the first level trigger to select events with high  $P_t$  electrons. This is followed by a hadron calorimeter (HCAL). The HCAL is used in the first level trigger to select events with relatively high  $P_t$  clusters to discriminate against minimum bias events and preferentially select  $B$  events. Muon chambers are positioned in front of the ECAL and are interleaved with iron absorbers behind the HCAL to create a muon detector at the end of the system. The muon system is designed to facilitate triggering on high- $P_t$  muons and dimuons from  $B$  decays[38].

The LHCb detector has all the necessary qualities to do the complete menu of  $B$  decays we described above. The detector is designed to handle high rate and large radiation levels associated with operation at luminosities of up to or beyond  $2 \times 10^{32}/\text{cm}^2\text{-s}$ .

**8.2.1. Triggering in LHCb.** The LHCb trigger is dedicated to selecting  $B$  decays[38]. It consists of three levels called Level 0, Level 1 and the High Level Trigger(HLT).

The Level 0 Trigger has three parts: 1) A Muon Trigger, to select high  $P_t$  muons and suppress backgrounds mainly from  $\pi$  and  $K$  decays. It employs the 5 muon cham-

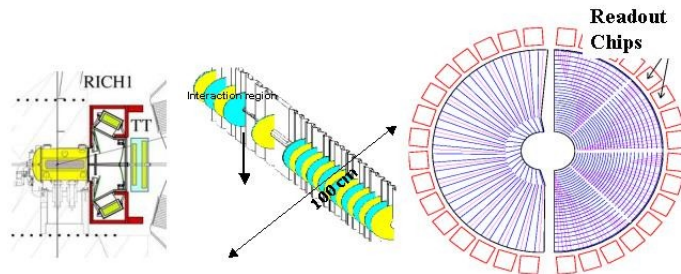


Fig. 25. – Schematic of VELO: the left side shows the vacuum vessel housing the VELO, located on the IR and just upstream of RICH1; the middle shows the layout of the disks; the right side shows the layout of the strips on the radial disk, which is used in the vertex trigger.

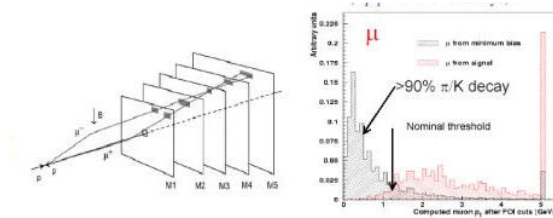


Fig. 26. – The left hand side shows schematically how the 5 stations of the LHCb muon chambers are used to reconstruct penetrating tracks and estimate their momentum by projecting back through the analysis magnet to the IP; the right hand side shows the source of the muons that are seen by the detector.

bers, M1-M5, to form tracks that have penetrated the steel absorbers and projects them through the magnet back to the IP. This projection technique provides an estimate of the momentum good to 20%. The system and the transverse momentum spectrum of muons are shown in Figure 26. A cut of about 1.25 GeV/c produces a clean sample of semi-muonic- $B$  decays. 2) A calorimeter trigger to select events with relatively large  $E_t$  using the ECAL and HCAL. The search is conducted in regions of  $2 \times 2$  cells. A threshold of 3 GeV is used. 3) A special set of tracking chambers, the Trigger Tracker just upstream of the first RICH to determine the number of primary interactions in the event (beam crossing) based on a fast tracking algorithm. The hits on the two chambers are used to produce a histogram of  $z$  intersections on the beam axis. Peaks in these histograms represent interaction vertices. This system is used to reject events with more than one primary interaction vertex.

The Level 1 trigger uses the VELO to reconstruct tracks and measure their impact parameter relative to the primary vertex. The VELO has 21 stations with alternating sensors with  $r$ - $\phi$  strip layout. The strip pitch varies from  $40 \mu\text{m}$  to  $100 \mu\text{m}$ . A fast tracking strategy using only the  $r$ - $z$  views, i.e. only the  $r$ -strips, is used to find the primary vertex. The resolution of the primary vertex is typically  $\sigma_z \sim 60 \mu\text{m}$  and  $\sigma_{x,y} \sim 20 \mu\text{m}$ . The next step is to select 2-dimensional projections of tracks with an impact parameter of 0.15 to 3 mm. Finally, a 3-dimensional fit is performed to confirm the impact parameter of certain selected candidates. The momentum of the track is estimated by extending the track into the “trigger tracker” system and observing the bend in fringe field of the large dipole. The kick of the fringe field is about  $\int B \times dl$  is about 0.15 T-m, giving a momentum resolution of 20-40%. VELO tracks are then linked to the Level 0 objects to form the trigger.

The final Level 1 trigger has three separate “lines”: Muon Lines, including single muons and dimuons; Photon, Electron lines; and Generic Lines, which select on general features of the vertex topology and the presence of high  $P_t$  particles.

The HLT is a farm of commercial microprocessors. They redo the Level 1 trigger with full resolution. For the surviving candidates, they do a full reconstruction using all the detectors and then form two streams: an Exclusive Stream consisting of events containing candidates from a list of exclusive final states; and an Inclusive Stream of “generic”  $B$  candidates based on the presence of “ $B$ ”-like properties.

The interaction rate is about 10 MHz. About 1 MHz survive Level 0. Level 1 selects 40KHz. The High Level Trigger produces the two streams mentioned above. This trigger

TABLE V. – *The Physics Reach of LHCb for integrated luminosity of  $2 \text{ fb}^{-1}$ .*

	channel	yield	precision
$\gamma$	$B_s \rightarrow D_s K$	5.4K	$\sigma(\gamma) \approx 14^\circ$
	$B_d \rightarrow \pi\pi; B_s \rightarrow KK$	26K, 37K	$\sigma(\gamma) \approx 6^\circ$
	$B_d \rightarrow D^0 K^*$	0.5K	$\sigma(\gamma) \approx 8^\circ$
	$B_d \rightarrow D^0 K^*$	3.4K	
	$B_d \rightarrow D_{CP} K^*$	0.6K	
$\chi$	$B_s \rightarrow J/\psi \phi$	120K	$\sigma(\chi) \approx 2^\circ$
$ V_{td}/V_{ts} $	$B_s \rightarrow D_s \pi$	80K	$\Delta M_s$ up to $68 \text{ ps}^{-1}$
Rare Decays	$B_d \rightarrow K^* \gamma$	35K	$\sigma(A_{CP}^{dir}) \approx 0.01$

results in a stream of “hot candidates” of about 200Hz and an archival stream of up to 2KHz.

**8.3. Physics Reach of LHCb.** – The physics reach of LHCb[36] is given in Table V. It includes precision measurements of  $B_d$  and  $B_u$  decays that improve on what can be done at existing  $e^+e^- B$  factories and even proposed “super  $B$  Factories” that might achieve luminosities of  $10^{36}/\text{cm}^2\text{-s}$ . It also includes high statistics studies of  $B_s$  decays,  $B_c$  and  $b$ -baryons. As a dedicated experiment, it comes closest to meeting the requirements set forth in section 5 for the next generation hadron collider  $B$  experiment.

## 9. – Outlook

CDF and  $D\mathcal{O}$  have overcome many of the challenges of doing  $B$  physics at hadron colliders. They have adequate vertex resolution to isolate signals and measure their proper time evolution. They have begun to address the trigger challenge. They are contributing to  $B_s$ ,  $\Lambda_b$ , and  $B_c$  physics, areas where they are complementary to studies at  $e^+e^-$  machines.  $B_s$  mixing and lifetime differences are major goals. However, their sensitivity in some studies suffers from inadequacies of the trigger and lack of particle identification and flavor tagging power. They may not become competitive with  $e^+e^-$  for  $B_d$  and  $B_u$  physics, except for rare decays containing muons, even with the full data set that will be available when their data-taking ends around 2009.

ATLAS and CMS are likely to carry out a high quality, somewhat limited menu of “general  $B$  physics” during the period of “low luminosity running”  $\sim 10^{33}/\text{cm}^2\text{-s}$  early in the LHC. They will be limited by lack of particle identification and triggering problems. At the full LHC luminosity of  $\sim 10^{34}/\text{cm}^2\text{-s}$ , the triggering problem will become very severe and radiation damage will degrade the performance of the vertex detectors.  $B$  physics studies will be limited to searches for very rare decays involving dimuons in the final state. For these rare decays, ATLAS and CMS should have excellent sensitivity.

LHCb will be the first “dedicated  $B$  experiment” at a hadron collider. It is designed to meet all the challenges for doing  $B$  physics, including high resolution vertex reconstruction, excellent mass and momentum resolution, sophisticated secondary vertex triggering with the trigger bandwidth completely committed to  $B$  physics, excellent particle identification, and good photon reconstruction. Operating with high efficiency at a luminosity of  $2 \times 10^{32}$ , it should be the dominant force in the full range of  $B$  physics, including  $B_s$ ,  $B_c$ ,  $\Lambda_b$  and  $B_d$  and  $B_u$ , where it should be competitive with a super- $B$  factory.

\* \* \*

This work was supported by the Fermi National Accelerator Laboratory, which is operated by Universities Research Association, Inc. under contract No. DE-AC02-76CH03000 with the United States Department of Energy.

The author wishes to thank the members of the BTeV and FOCUS Collaborations from which he has learned much and to thank Guennadi Borissov and Rick Van Kooten of D0 and Matthew Herndon and Stefano Giagu of CDF for help in preparing talk. He also thanks the organizers of the Fermi School for providing an excellent conference in a beautiful setting

## REFERENCES

- [1] See, for a recent summary,  
<http://lp2005.tsl.uu.se/lp2005>, or  
<http://www.pg.infn.it/beauty2005/conferenceprogram.htm>.
- [2] N. Cabibbo, *Phys. Rev. Lett.* **10** (1963) 531; M. Kobayashi and K. Maskawa, *Prog. Theor. Phys.* **49** (1973) 652.
- [3] L. Wolfenstein, *Phys. Rev. Lett.* **51** (1983) 1945.
- [4] R. Aleksan, B. Kayser, and D. London, *Phys. Rev. Lett.* **73** (1994) 18.
- [5] see, for results at the time of this talk:  
<http://www.slac.stanford.edu/xorg/hfag/triangle/summer2005/index.shtml>.
- [6] A. Giri, Y. Grossman, A. Soffer, and J. Zupan, *Phys. Rev.* **D68** (2003) 054018; M. Gronau and D. Wyler, *Phys. Lett.* **B265** (1991) pp. 172-176; M. Gronau and D. London, *Phys. Lett.* **B253** (1991) pp. 483-488; and D. Atwood, I. Dunietz, and A. Soni, *Phys. Rev. Lett.* **78** (1997) pp. 3257-3260.
- [7] J. P. Silva and L. Wolfenstein, *Phys. Rev.* **D55** (1997) 5331.
- [8] R. Aleksan, B. Kayser, D. London, *Phys. Rev. Lett.* **73** (1994) pp. 18-20
- [9] For the latest compilation, see  
<http://www.slac.stanford.edu/xorg/hfag/triangle/summer2005/index.shtml#qqqs>.
- [10] A. Ali, P. Ball, L.T. Handoko, G. Hiller, *Phys. Rev.* **D61** (2000) 074024.
- [11] CDF collaboration, F. Abe et al., Measurement of the  $B$  meson differential cross-section,  $d\sigma/dP_T$ , in  $p\bar{p}$  collisions at  $\sqrt{s}=1.8$  TeV, *Phys. Rev. Lett.* **75** (1995) 1451; and CDF collaboration, D. Acosta et al., Measurement of  $B^+$  total cross-section and  $B^+$  differential cross-section,  $d\sigma/dP_T$ , in  $p\bar{p}$  collisions at  $\sqrt{s}=1.8$  TeV, *Phys. Rev.* **D65** (2002) 052005.
- [12] DØ collaboration, S. Abachi et al., Inclusive  $\mu$  and  $B$  quark production cross-section in  $p\bar{p}$  collisions at  $\sqrt{s}=1.8$  TeV, *Phys. Rev. Lett.* **74** (1995) 3548; DØ collaboration, B. Abbott et al., Small angle muon and bottom quark production in  $p\bar{p}$  collisions at  $\sqrt{s}=1.8$  TeV, *Phys. Rev. Lett.* **84** (2000) 5478; DØ collaboration, B. Abbott et al., The  $b\bar{b}$  cross-section and angular correlation in  $p\bar{p}$  collisions at  $\sqrt{s}=1.8$  TeV, *Phys. Lett.* **B487** (2000) 264; and DØ collaboration, B. Abbott et al., Cross-section for  $B$  jet production in  $p\bar{p}$  collisions at  $\sqrt{s}=1.8$  TeV, *Phys. Rev. Lett.* **85** (2000) 5068.
- [13] Matteo Cacciari et al., *J. High Energy Phys. JHEP07* (2004) 033.
- [14] The CMS collaboration, *CMS Physics Technical Design Report, Volume II, draft version of November 3, 2005*, p86.
- [15] D. Fein, *Tevatron Results on b-Quark Cross Sections and Correlations*, FERMILAB-Conf-99/050-E, published in the Proceedings of the 13th Topical Conference on Hadron Collider Physics, Mumbai, India, January 14-20, 1999; and  
<http://www.physics.mcgill.ca/royp/andreas.pdf>.
- [16] Documentation for Pythia may be found at  
<http://www.thep.lu.se/torbjorn/Pythia.html>.
- [17] Penelope Kasper, *CP Violation in  $B_s \rightarrow D_s K$* , BTeV internal note #55, 1997.
- [18] S. Barsuk, *The LHCb experiment: Status and expected physics performance*, presented at Beauty05, Assisi, June 20-24, 2005.

- [19] E. Eichten, C.T. Hill. and C. Quigg, *Phys. Rev. Lett.* 71, (1993) pp. 4116-4119; and *B Physics at the Tevatron: Run II and Beyond*, FERMLAB-Pub-01/197, pp. 82-86.
- [20] A good source of material is The ROSE Collaboration, CERN RD48, whose homepage is <http://rd48.web.cern.ch/RD48>.
- [21] J.N. Butler, *Triggering and Data Acquisition*, First Instrumentation School/Workshop at the Instrumentation Center in Morelia, Mexico, 2002.
- [22] see, for example,  
<http://www-cdf.fnal.gov/physics/new/bottom/bottom.html>  
 and <http://www-d0.fnal.gov/Run2Physics/WWW/results/b.htm>.
- [23] M. Rescigno, *B Mixing at CDF*, invited talk at Beauty05, Assisi, Italy 2005. For the CDF time-of-flight system, see  
[http://www.physics.purdue.edu/jones105/tof/cdf\\_tof.ppt](http://www.physics.purdue.edu/jones105/tof/cdf_tof.ppt)  
 and <http://www.ifca.unican.es/imfp03/IVila.ppt>
- [24] T. Bellunato, *Status of the LHCb RICH detector and the HPD*, invited talk at Beauty05, Assisi, Italy 2005.
- [25] Mauro Dell'Orso, *The CDF Silicon Vertex Trigger*, invited talk at Beauty05, Assisi, Italy, 2005; A. Bardo et al., *Nucl. Instrum. Meth.* **A485** (2000) pp. 178-182; and B. Ashmankas et al., *Nucl. Instrum. Meth.* **A518** (2004) pp. 532-536.
- [26] E.J. Thomson et al., Online Track Processor for the CDF Upgrade, *IEEE Trans. Nucl. Sci.* 44 (2002) pp. 1063-1070.
- [27] D. Acosta et. al, the CDF collaboration, *Phys. Rev. Lett.* 94 (2005) 101803.
- [28] Rick Jesik, *B Lifetimes and Mixing at the Tevatron*, invited talk at Lepton Photon 2005, Uppsala, Sweden, June 30-July 5, 2005.
- [29] Masashi Tanaka, *CDF Results on B Physics*, invited talk at The Tevatron Connection Workshop, Fermilab, June 24, 2005.
- [30] A useful reference with plots on the trigger performance may be found at [http://www-d0.fnal.gov/Run2Physics/public/ICHEP2002\\_Levan.ppt](http://www-d0.fnal.gov/Run2Physics/public/ICHEP2002_Levan.ppt)
- [31] V.M. Abazov et al., *The Muon System of the Run II DØ Detector*, Fermilab PUB-05-034-E, 2005.
- [32] Hal Evans, *B Physics at DØ: Recent Results and Plans*, invited talk, The Tevatron Connection Workshop, Fermilab, June 24, 2005.
- [33] Ch. Petridou, *b-Physics expectations at ATLAS and CMS*, invited talk at Beauty05, Assisi, Italy 2005.
- [34] Natalia Panikashvili, *The ATLAS B physics trigger*, invited talk at Beauty 2005, Assisi, Italy 2005.
- [35] F. Schilling, *Prospects of measuring  $B_s \rightarrow \mu^+ \mu^-$  with CMS*, invited talk at Beauty05, Assisi, Italy 2005.
- [36] S. Barsuk, *The LHCb experiment: Status and expected physics performance*, invited talk at Beauty05, Assisi, Italy 2005.
- [37] M. Needham, *Status and Expected Performance of the LHCb Tracking System*, invited talk at Beauty05, Assisi, Italy 2005.
- [38] F. Teubert, *LHCb Trigger System*, invited talk at Beauty05, Assisi, Italy 2005.